



Modelling of combined Navier–Stokes and Darcy flows in crossflow membrane filtration

V. Nassehi*

Chemical Engineering Department, Loughborough University, Loughborough LE11 3TU, U.K.

(Received 12 May 1997 and accepted in revised form 10 December 1997)

Abstract—Computer simulation of the flow field in crossflow membrane filtration in a porous tube and shell system depends on the imposition of permeable wall conditions on the surface of the inner tube. Porous wall conditions are often represented by the Darcy equation which relates the pressure gradients within a flow stream to the flow rates through the permeable walls of the flow domain. In crossflow filtration the feed stream which flows tangentially to the porous tube surface is modelled by the Navier–Stokes equations. These equations represent viscous laminar Newtonian flow. They can also be generalised to deal with non-elastic, non-Newtonian fluids. The existence of viscous stress terms in the Navier–Stokes equations, which are expressed in terms of second-order partial derivatives, makes the straightforward linking of these equations to the Darcy equation in a numerical solution scheme impossible. Therefore, in order to develop a fluid dynamical model for crossflow filtration, special techniques which resolve this difficulty must be used. In this paper first, various methods of linking the Navier–Stokes and the Darcy equations in a solution scheme are considered and the strength and weaknesses of these methods are discussed. Following this discussion the details of a novel method which is used to develop a robust, accurate and cost-effective finite-element simulation scheme for the combined Navier–Stokes/Darcy flows in crossflow filtration is presented. © 1998 Elsevier Science Ltd. All rights reserved.

Keywords: Crossflow filtration; porous boundaries; Navier–Stokes equations; Darcy equation; modelling; finite-element method.

INTRODUCTION

The combination of free flow and flow through porous media occurs in a wide range of fluid processes such as crossflow and deadend filtration, viscous flow over a bed of solid particles and solidification of metal alloy melts during moulding. However, despite the superficial similarity of the flow regimes in these processes underlying flow field characteristics can vary significantly from one type of process to another. For example, in some operations, there is a constant and distinct interfacial boundary between the free flow domain and the porous media. In other cases the shape and the position of the interface between these zones change continuously by the progress of the process. Other factors such as fluid compressibility, flow Reynolds number, type of pores and porosity of porous media also directly affect the dynamics of the combined flows. The diversity of underlying phenomena and the complexity of interactions between

free and porous flow systems have prevented generalised theoretical analysis of the coupled flow systems. Fluid dynamical description of free flows usually do not cause a problem and in great majority of instances the well-known Navier–Stokes equations can be used to model these sections. The main difficulty, in mathematical terms, is the formulation of fluid flow equations which can reliably represent both the interfacial boundary and the flow through porous section in all types of combined flows. However, mathematical models which justifiably represent coupled free and porous flows under specific conditions can be developed. These models provide useful predictive tools for the investigation and design of important classes of combined flow processes.

The validity of the Darcy's law for the representation of viscous, laminar, incompressible flows in porous media with small porosity is widely accepted (Beavers and Joseph, 1967; Gartling *et al.*, 1997). Therefore, in processes that a combined free and porous flow occurs under the stated conditions the flow regime must be modelled by the coupling of the Darcy and the Navier–Stokes equations. The

*Tel.: 01509 222522; fax: 01509 223923; e-mail: v.nassehi@lboro.ac.uk.

important point is to make sure that, wherever necessary, the continuity of flow field variables across the interface between free flow and porous region is maintained.

The absence of the second-order derivatives in the Darcy model is often cited as a source of difficulty in coupling the Navier–Stokes and Darcy equations. The substitution of the Darcy model with an alternative equation which includes second-order derivatives apparently resolves this difficulty. However, in processes where there is no experimental or theoretical justifications for the substitution of the Darcy equation with a different model such an approach cannot be used. The main focus of the present study has been the development of a scheme for the imposition of permeable wall conditions in viscous flow domains which can resolve the difficulties associated with the existing techniques of coupling the Darcy and Navier–Stokes regimes. In this paper the developed method in the context of a finite-element model for an isothermal, steady-state laminar flow of a homogeneous power-law fluid in an annular domain with a permeable inner wall is described. It is shown that this scheme can be successfully used to model the combined flow field in crossflow filtration processes.

Crossflow membrane filtration is one of the most important separation techniques used in process industries. Different configurations and design specifications can be used to construct industrial crossflow filtration systems. Fundamentally, however, an axisymmetric crossflow filter is described as an annulus in which a fluid (e.g. a suspension of fine particles or a solution) flowing parallel to the axis of the symmetry of the annulus permeates through the porous walls of the inner tube in the radial direction. The porous inner tube is made of a material which displays different permeability against the fluid and particles (or solvent and solute in solutions) and therefore acts as a membrane, separating the constituents of the feed stream fluid. An overview of the process has been published by Gutman (1987) and other numerous works dedicated to the analysis, modelling, characterisation and classification of crossflow filters can also be found in the literature. Generally, crossflow filtration is described as a complex time-dependent operation and a complete mathematical model for this process should include appropriate transport, constitutive and fluid dynamical equations. However, the type and nature of the mechanisms which determine the physical characteristics of filtration processes depend on various factors such as the duration of the operation, properties of the feed stream fluid and the size distribution of the solid particles in slurries and suspensions. Therefore, it is not possible to develop a universally applicable mathematical model for all types of crossflow filtration and the particular characteristics of each process should be appropriately included in the set of the governing equations which represent that process. On the other hand, the underlying fluid dynamical behaviour of almost all types of crossflow filtration processes can be mathematically

described by a common form. It should be noted, however, that despite this commonality the solution of the fluid dynamical equations on their own cannot provide practical process analysis data. This is due to the following factors. As the filtration progresses the physical characteristics of the fluid being filtered, such as its density and viscosity distributions, change. Furthermore, the mutual interactions of solid particles in the suspension with each other and the fluid continuum continuously vary affecting the balance of the forces in the flow domain. Therefore, the rate and the mode of the transport of the solids in crossflow filtration and the fluid dynamical behaviour of these systems should be treated as interdependent. In addition, due to the deposition of the solid particles on the surface of the inner tube and the fouling of the porous wall the permeability of the membrane varies during the process. Also in some cases the narrowing of the annular cross-section, caused by the deposition of the solids, can be significant and therefore it may be necessary that the changing geometry of the flow domain should be taken into account. In most cases, however, a pseudo-equilibrium condition prevails after some time and from then on the filtration may be considered as a steady-state process (Bowen *et al.*, 1996). Despite the importance of the above-described mechanisms the necessity of the imposition of the permeable wall conditions remains the most essential and basic requirement in modelling of the flow regime in crossflow filtration. Thus, the fulfilment of this requirement is the prerequisite of any acceptable mathematical simulation of crossflow filtration. Moreover, it is self-evident that the validity and effectiveness of the method used to couple free and porous flow equations will not be compromised by making simplifying assumptions about the other physical characteristics of the process. In this study, the flow field in crossflow membrane filtration is modelled by the coupling of the Navier–Stokes and Darcy equations. This model is particularly valid for track-etched membranes which have low porosity. Quantitative evaluations based on overall mass balance are used to validate the simulations obtained using the developed scheme.

GOVERNING EQUATIONS

Consider steady-state, laminar, isothermal flow of a homogeneous suspension in an axisymmetric annular domain with a permeable inner wall. The flow regime in this domain is described by the following set of equations.

(I) The continuity equation, expression of overall mass balance for an incompressible fluid flow:

$$\frac{\partial v_r}{\partial r} + \frac{v_r}{r} + \frac{\partial v_z}{\partial z} = 0 \quad (1)$$

where r and z are the radial and axial coordinates, respectively, and v_r , v_z are the velocity components.

(II) The equation of motion (components of the Navier–Stokes equations), expression of momentum

balance for an incompressible fluid flow:

$$\begin{aligned} \rho v_r \frac{\partial v_r}{\partial r} + \rho v_z \frac{\partial v_r}{\partial z} + \frac{\partial p}{\partial r} - \frac{\partial}{\partial r} \left(2\eta \frac{\partial v_r}{\partial r} \right) - \frac{2\eta}{r} \frac{\partial v_r}{\partial r} \\ + \frac{2\eta v_r}{r^2} - \frac{\partial}{\partial z} \left[\eta \left(\frac{\partial v_z}{\partial r} + \frac{\partial v_r}{\partial z} \right) \right] - \rho g_r = 0 \\ \rho v_r \frac{\partial v_z}{\partial r} + \rho v_z \frac{\partial v_z}{\partial z} + \frac{\partial p}{\partial z} - \frac{\partial}{\partial z} \left(2\eta \frac{\partial v_z}{\partial z} \right) - \frac{\eta}{r} \left(\frac{\partial v_z}{\partial r} + \frac{\partial v_r}{\partial z} \right) \\ - \frac{\partial}{\partial r} \left[\eta \left(\frac{\partial v_z}{\partial r} + \frac{\partial v_r}{\partial z} \right) \right] - \rho g_z = 0 \end{aligned} \quad (2)$$

where ρ is the fluid density, p the pressure and ρg_r , ρg_z are the components of the body force. In the present analysis, the shear dependent viscosity of the suspension, η , is defined by the following power-law relationship.

$$\eta = \eta_0 \dot{\gamma}^{n-1} \quad (3)$$

where η_0 is the zero shear viscosity (consistency coefficient), $\dot{\gamma}$ is the shear rate and n is the power-law index.

BOUNDARY CONDITIONS

In the present work the above-described governing equations are solved subject to the following boundary conditions. At the inlet the feed stream velocity is defined. The outer shell provides non-slip solid walls and the velocity components on this surface are equal to zero. The inner wall is permeable and the following Darcy equations are used to describe the conditions on this surface:

$$\begin{aligned} \frac{\mu_f}{K_r} v_r + \frac{\partial p}{\partial r} = 0 \\ \frac{\mu_f}{K_z} v_z + \frac{\partial p}{\partial z} = 0 \end{aligned} \quad (4)$$

where μ_f is the viscosity of the filtrate (assumed to be constant) and K_r , K_z are the porous wall permeability coefficients in radial and axial directions, respectively. Equations (4) also describe the flow of the filtrate through the porous wall of the inner tube. The filtrate flow inside the inner tube can be described by a set of equations similar to eqs (1) and (2).

It is well known that the imposition of artificial no-flux (stress free) exit conditions may lead to unacceptable numerical errors in flow simulations. A method suggested by Papanastasiou *et al.* (1992) which is based on apparently imposing no outlet boundary conditions is mathematically proved to lead to the prescription of an effective proper boundary condition at the exit section for Navier–Stokes equations (Renardy, 1997). In the present work, either this method is used or a non-permeable section is added to the end of the porous wall and the exit is considered to be at the end of this section. The imposition of the developed flow conditions at the exit from the free flow domain in the latter case is found to give very accurate results.

FINITE-ELEMENT SOLUTION OF THE GOVERNING EQUATIONS

The power and flexibility of the finite-element method in dealing with non-linear field problems in geometrically complex domains make this technique the most appropriate method for the solution of the governing equations of viscous flows. In particular, the weighted residual Galerkin finite-element schemes (Zienkiewicz and Taylor, 1994) have been extensively used in conjunction with C^0 continuous simplex and tensor product Lagrangian elements to solve a variety of industrial problems (Reddy and Gartling, 1994; Tucker, 1989; Nassehi, 1996). However, in the case of a viscous flow in a domain with permeable walls a routine and straightforward solution scheme based on the use of C^0 elements cannot be developed. This difficulty stems from the inability of the C^0 elements to cope with the second-order derivatives in the governing equations of the flow problem. To resolve this complication, ordinarily, the Green's theorem (analogous to integration by parts) is used to reduce the order of the second-order differentials in the finite element formulation of viscous flows. This treatment results in the appearance of additional terms in the finite element equations representing viscous stress flux across the element boundaries, such as

$$\int_{\Gamma} \left(2\eta \frac{\partial v_r}{\partial r} n_r \right) d\Gamma, \quad \text{etc.} \quad (5)$$

where Γ is the elemental boundary surface and n_r is the radial component of the unit vector normal (in the outward direction) to the element boundary. Normally, it can be assumed that along the shared internal elemental boundaries in the solution mesh for every flux term, from one side, there will be an equivalent term with opposite sign, from the other side, generated by the application of the Green's theorem to the model equations written for an adjacent element. Therefore, during the assembly of the elemental equations all such terms will be cancelled out. Furthermore, on the exterior boundaries of the flow domain the imposition of essential or natural boundary conditions will make the use of governing equations redundant and hence there is no need for any special treatment of the flux terms on the exterior boundaries. It is thus clear that a viscous flow combined by flow through porous media in which the two parts are represented by different flow equations (i.e. Navier–Stokes and Darcy) cannot be modelled by a technique based on the routine application of the Green's theorem. Such a treatment will result in the generation of additional flux terms along the boundary joining the Navier–Stokes/Darcy regimes which cannot be assumed to disappear during the assembly of the elemental equations. Typical examples of the previously developed techniques which aim to solve this problem are as follows.

Pangrle *et al.* (1991) avoided the above-described difficulty in modelling laminar flow in porous tube

and shell systems by assuming that the flow at the interface between a porous medium and free fluid can be represented by the Brinkman equation instead of the Darcy equation. The Brinkman (1947) equation is written as

$$\nabla p - \mu^* \nabla^2 \underline{v} = -\frac{\mu}{K} \underline{v} \quad (6)$$

where μ^* is defined as the effective viscosity of the fluid flowing through the porous wall. Theoretical studies show that the validity of the Brinkman equation is limited to very high porosity domains (Lundgren, 1972; Kim and Russell, 1985). However, as it can be seen from eq. (6) this model contains second-order derivatives of the velocity. Thus, if it is assumed that the effective viscosity of the filtrate is the same as the viscosity of the suspension in the feed stream the application of the Green's theorem to eq. (6) results in the generation of flux terms which cancel out their counterpart terms in the free fluid domain during the assembly procedure. In general, this assumption cannot be supported by theoretical or experimental analyses (Kaviany, 1991; Martys *et al.*, 1994; Givler and Altobelli, 1994) and Pangrle *et al.* (1991) point out that the use of the Brinkman equation in the described form only provides a qualitative solution for the flow in shell and porous tube systems. An analysis of the limits of the applicability of the Brinkman equation for flow in porous media is reported by Durlofsky and Brady (1987). It is also self-evident that in the cross-flow filtration of suspensions, the effective viscosity of the filtrate passing through the porous wall cannot be equal to the viscosity of the feed stream fluid being filtered.

Nassehi and Petera (1994) developed a method for the solution of the combined Navier–Stokes/Darcy flow problems which is based on the use of least-squares finite-element method. In this scheme, C^1 continuous isoparametric Hermite elements are used. Hermite elements are constructed utilising higher-order interpolation models and therefore they can automatically cope with second-order derivatives in the governing differential equations without using the Green's theorem. However, more detailed numerical experiments using this new element showed that the developed least-squares scheme has the following shortcomings. The number of degrees of freedom in the solution domain increases very rapidly by mesh refinement and consequently the use of the Hermite elements requires excessive computational effort. This problem becomes particularly acute in three-dimensional filtration flow simulations. Second, in the least-squares scheme the Green's theorem is not used and this means that in non-Newtonian flows the shear-dependent viscosity appearing in the viscous stress terms remains subject to differentiation. It is therefore necessary to calculate the derivatives of the viscosity at the integration points in this scheme. The inaccuracy resulting from the approximate numerical differentiation of viscosity function was found to be

significant in the simulation of practical shell and porous tube systems. Another requirement of the described least-squares scheme is that the entire domain consisting of the free flow in the outer annulus, the flow through the inner tube wall and the free flow of the permeate inside the inner tube should always be modelled in a coupled form. Thus, the scheme lacks the flexibility of being used in a form in which the Darcy equation is imposed simply as a boundary condition along a permeable wall in viscous flow domains.

In order to resolve the above-described problems, a Galerkin finite-element scheme for the combined Navier–Stokes/Darcy flow based on the use of C^0 Lagrange elements is developed by Nassehi and Petera (1997). In this scheme, the layer of the elements joining the porous wall to the rest of the domain in the solution mesh are formulated in a form which can represent a combined flow field. Essentially, this is achieved by replacing the terms of the elemental stiffness equations which correspond to the nodes located on the porous surface by the discretised form of the appropriate Darcy components while letting the remaining terms in these matrices to remain the same as those originating from the Navier–Stokes equations. In cases where a model for the whole system of outer shell, porous wall and inner tube is required a similar layer of elements combining the Darcy and the Navier–Stokes equations are used to join the flow domain inside the inner tube to the inner surface of the porous wall. In order to obtain stable numerical results for incompressible flow the Ladyzhenskaya–Babuska–Brezzi (LBB) condition must be satisfied (Reddy, 1986). This poses a severe restriction on the choice of elements which can be used in the described scheme. This is due to the representation of incompressibility constraint via eq. (1) in this approach. The most convenient element to be used is the C^0 continuous Taylor–Hood element (Taylor and Hood, 1973) which is based on a lower order of interpolation for the pressure calculations than the velocities. Thus, despite the success of this scheme in dealing with the basic problem associated with the coupling of the Darcy and Navier–Stokes equations due to the inevitable reduction in the accuracy of the pressure interpolation it introduces an additional approximation into the flow simulations. Furthermore, restrictions in the choice of approximations for the velocity and pressure results in a scheme which cannot be clearly shown to lead to a convergent solution under all conditions for a combined Navier–Stokes/Darcy flow (Gartling *et al.*, 1997). It can be argued that the ability to yield very accurate and continuous pressure values on the porous wall surface is crucial in determining the usefulness of a combined scheme of this kind. To achieve this objective in the present work an alternative method for the fulfilment of the incompressibility constraint is used. In this method instead of a divergence free velocity field [i.e. equation (1)] the following equation which, theoretically, represents slightly compressible fluids

is used:

$$\frac{1}{c^2} \frac{\partial p}{\partial t} + \rho \left(\frac{\partial v_r}{\partial r} + \frac{v_r}{r} + \frac{\partial v_z}{\partial z} \right) = 0 \tag{7}$$

where c is the speed of the sound in the fluid. The use of eq. (7) to model incompressible flow with equal-order interpolation functions for velocity and pressure in the finite-element solution schemes which satisfy the LBB condition without any complications is very well established (Zienkiewicz and Wu, 1991). In the present scheme to make all of the model equations compatible with eq. (7) appropriate time-dependent inertia terms such as $\rho(\partial v_r/\partial t)$ are added to the left-hand sides of the components of the Navier–Stokes equation (2) and the Darcy equation (4). Zienkiewicz and Wu (1991) give a detailed description of various finite-element discretisations which can be used to obtain stable and accurate solutions for incompressible viscous flow using equal-order interpolation for velocity and pressure in models which are based on eq. (7) instead of the usual incompressibility constraint. They further show that this approach can be very conveniently applied to obtain steady-state results iteratively using a transient computational scheme.

WORKING EQUATIONS OF THE NEW SCHEME

The temporal derivatives in the model equations are first treated using a two-level time-stepping scheme (Nassehi and Bikangaga, 1993). In this scheme, the predictor step to time level $t^{n+1/2}$ is given as

$$\rho \frac{\partial v_r^e}{\partial t} \Big|_n = \rho \frac{v_r^e|^{n+1/2} - v_r^e|_n}{\Delta t_n/2} \tag{8a}$$

$$\rho \frac{\partial v_z^e}{\partial t} \Big|_n = \rho \frac{v_z^e|^{n+1/2} - v_z^e|_n}{\Delta t_n/2} \tag{8b}$$

$$\frac{\partial p^e}{\partial t} \Big|_n = \frac{p^e|^{n+1/2} - p^e|_n}{\Delta t_n/2} \tag{8c}$$

where v_r^e , v_z^e and p^e are trial function representations of the velocity components and pressure, respectively, which in the context of the finite-element discretisations are found within each element in terms of the interpolation functions as

$$v_r^e = \sum_{m=1}^k N_m v_r^m \tag{9a}$$

$$v_z^e = \sum_{m=1}^k N_m v_z^m \tag{9b}$$

$$p^e = \sum_{m=1}^{k'} N_m p^m \tag{9c}$$

where v_r^m , v_z^m and p^m are the nodal values of the components of the velocity and pressure, respectively, N_m is the interpolation function associated with node number m in an element and k and k' are the number of velocity and pressure nodes per element. As ex-

plained in the previous section in the present scheme, elements which are based on equal degrees of interpolation for velocity and pressure are used. The following corrector step generates solution at time level t^{n+1} ,

$$\rho \frac{\partial v_r^e}{\partial t} \Big|^{n+1/2} = \rho \frac{v_r^e|^{n+1} - v_r^e|_n}{\Delta t_n} \tag{10a}$$

$$\rho \frac{\partial v_z^e}{\partial t} \Big|^{n+1/2} = \rho \frac{v_z^e|^{n+1} - v_z^e|_n}{\Delta t_n} \tag{10b}$$

$$\frac{\partial p^e}{\partial t} \Big|^{n+1/2} = \frac{p^e|^{n+1} - p^e|_n}{\Delta t_n} \tag{10c}$$

After the replacement of the temporal derivatives in the model equations by relationships (8a)–(8c) and (10a)–(10c), the finite element discretisation is carried out. The spatial discretisation in the above-described predictor and corrector steps are based on the well-known weighted residuals Galerkin finite-element method (Zienkiewicz and Taylor, 1994). In this method, the residuals generated by the substitution of the variables in the model equations from relationships (9a)–(9c) are first weighted using weight functions identical to the interpolation functions and are then integrated over the element domain Ω^e . In these weighted residual statements the application of Green’s theorem (analogous to integration by parts) to the terms which involve second-order derivatives of velocity and, for reason of compatibility, first-order derivatives of pressure gives the working equations of the present scheme. Using matrix notations these equations are

Predictor step:

$$\begin{bmatrix} a_{lm_{11}} & a_{lm_{12}} & a_{lm_{13}} \\ a_{lm_{21}} & a_{lm_{22}} & a_{lm_{23}} \\ a_{lm_{31}} & a_{lm_{32}} & a_{lm_{33}} \end{bmatrix} \begin{Bmatrix} v_r^m \\ v_z^m \\ p^m \end{Bmatrix}^{n+1/2} = \begin{Bmatrix} b_{l1} \\ b_{l2} \\ b_{l3} \end{Bmatrix} \tag{11}$$

where

$$a_{lm_{11}} = a_{lm_{22}} = \int_{\Omega^e} \left(\frac{2\rho N_l N_m}{\Delta t_n} \right) r^e dr dz,$$

$$a_{lm_{33}} = \int_{\Omega^e} \left(\frac{2 N_l N_m}{\rho c^2 \Delta t_n} \right) r^e dr dz,$$

and $a_{lm_{12}}$, etc. the off-diagonal terms are all equal to zero. The weight functions, N_l ($l = 1, k$) are the same as the interpolation functions. In the present work isoparametric elements are used and therefore

$$r^e = \sum_{m=1}^k N_m r^m \quad \text{and} \quad z^e = \sum_{m=1}^k N_m z^m.$$

In conjunction with the above mapping relationships the measure of integration in the above formulations are transformed in the usual manner using the Jacobian of coordinate transformations (Zienkiewicz and Taylor, 1994). The terms of the load vector (right-hand side) in eq. (11) represent values at time level

t^n and we have, for example,

$$\begin{aligned}
 b_{l_1} = & \left\{ \int_{\Omega_e} - \left[- \frac{2\rho N_l N_m}{\Delta t_n} \right. \right. \\
 & + N_l \left(\rho v_r^e \frac{\partial N_m}{\partial r} + \rho v_z^e \frac{\partial N_m}{\partial z} \right) \\
 & + 2\eta \frac{\partial N_l}{\partial r} \frac{\partial N_m}{\partial r} + 2 \frac{\eta}{r^2} N_l N_m + \eta \frac{\partial N_l}{\partial z} \frac{\partial N_m}{\partial z} \left. \right] \\
 & \times r^e dr dz \left. \right\} v_r^{m|n} + \left[\int_{\Omega_e} - \left(\eta \frac{\partial N_l}{\partial r} \frac{\partial N_m}{\partial r} \right) \right. \\
 & \times r^e dr dz \left. \right] v_r^{m|n} \\
 & + \left[\int_{\Omega_e} - \left(- \frac{\partial N_l}{\partial r} N_m - \frac{N_l N_m}{r^e} \right) \right. \\
 & \times r^e dr dz \left. \right] p^{m|n} + \int_{\Omega_e} N_l \rho g_r r^e dr dz \\
 & + \int_{\Gamma_e} N_l \left(2\eta \frac{\partial v_r^e}{\partial r} \right)^n n_r + \eta \frac{\partial v_r^e}{\partial r} \Big|^n n_z \\
 & + \eta \frac{\partial v_z^e}{\partial r} \Big|^n n_z - p^{e|n} n_r \Big) r^e d\Gamma_e \quad (12)
 \end{aligned}$$

where Γ_e is the element boundary and n_r and n_z are the components of the unit vector normal to the element boundary in outward direction. Other members of the load vector are analogous to the above example. The boundary integrals (i.e. the flux terms generated by the application of the Green's theorem) in equations corresponding to elements which are inside the free flow region are eliminated during the assembly of the elemental equations except for the layer which is on the porous wall surface. In this layer of elements the members of elemental equation (11), which correspond to the nodes located on the porous boundary, are substituted by the Darcy flow equations. Spatio-temporal discretisation of the Darcy flow equations, carried out in a similar way, yields a matrix equation whose left-hand side is identical to eq. (11); however, the members of the load vector (right-hand side) in this equation are derived as

$$\begin{aligned}
 b_{l_1} = & \int_{\Omega_e} \left[\left(\frac{2\rho}{\Delta t_n} - \frac{\mu_f}{K_r} \right) N_l N_m r^e dr dz \right] v_r^{m|n} \\
 & + \int_{\Omega_e} \left(\frac{\partial N_l}{\partial r} N_m r^e dr dz \right) p^{m|n} \\
 & - \int_{\Gamma_e} N_l p^{e|n} n_r r^e d\Gamma_e \quad (13a)
 \end{aligned}$$

$$\begin{aligned}
 b_{l_2} = & \int_{\Omega_e} \left[\left(\frac{2\rho}{\Delta t_n} - \frac{\mu_f}{K_r} \right) N_l N_m r^e dr dz \right] v_r^{m|n} \\
 & + \int_{\Omega_e} \left(\frac{\partial N_l}{\partial r} N_m r^e dr dz \right) p^{m|n} \\
 & - \int_{\Gamma_e} N_l p^{e|n} n_r r^e d\Gamma_e \quad (13b)
 \end{aligned}$$

$$\begin{aligned}
 b_{l_3} = & \int_{\Omega_e} - \left[\left(N_l \frac{\partial N_m}{\partial r} + N_l \frac{N_m}{r^e} \right) r^e dr dz \right] v_r^{m|n} \\
 & - \int_{\Omega_e} \left(N_l \frac{\partial N_m}{\partial z} \right) r^e dr dz v_z^{m|n} \\
 & + \int_{\Omega_e} \left(\frac{2N_l \partial N_m}{\rho c^2 \Delta t_n} r^e dr dz \right) p^{m|n}. \quad (13c)
 \end{aligned}$$

The line (boundary) integrals in eqs (13a) and (13b) cannot be neglected since this will amount to the wrong imposition of zero pressure along the permeable wall.

In practice, the modification of the working equations in the free flow region for elements which are adjacent to the permeable wall can be achieved in a number of ways. An apparently simple method is to use a thin layer of specially defined wall elements along the interface over which stiffness equations representing free flow and porous flow can be cast in appropriate forms and assembled. The problem with this approach is that these elements normally have very high aspect ratios and hence their use generates computational errors. An alternative method is to use a Lagrange multiplier technique in which wall conditions are imposed via the minimisation of a specially constructed functional (Zienkiewicz and Taylor, 1989). However, one cannot be sure that the described minimisation will always result in finding a suitable multiplier and the final set of equations to be solved may become highly ill-conditioned. To avoid these problems in the present scheme, a more direct approach for combining the working equations of free flow and porous regions is used. In this method, first the nodes which are located on the interface between two flow regions are identified and recorded. Then in the elemental stiffness equations obtained for the free flow region [i.e. equations found using working equation (11)] rows corresponding to the recorded degrees of freedom are substituted by the discretised form of the porous flow model [found using working equations (13a)–(13c)]. Since the interface nodes are common between the free and porous flow regions, the described modified elemental equations are assembled with their counterparts on the porous region over these common degrees of freedom. This ensures the continuity of the flow field variables across the interface.

Corrector step: The derivation of the working equations for this step is very similar to the predictor step and the final equations which are used to obtain the solution at time level $n + 1$ are analogous to the above-described working relationships. In the present application of the scheme where the steady-state solutions are required time stepping is based on an iterative cycle which is terminated after a satisfactory convergence is obtained.

The described scheme is very flexible and can also be employed to model a combined flow system in which the interface between two regions is not constant and changes by the progress of the process. In

this case at the end of every time step, after finding the new position of the moving boundary by a surface tracking procedure (e.g. see Petera and Nassehi, 1996), the new interfacial nodes are identified and the modified elemental equations are assembled over these nodes.

The developed scheme can also be used to model flow through porous regions bounded by solid walls. In this case solid walls are represented as impermeable interfaces and in the Darcy equation, k_r , k_z are set to be zero (to avoid division by zero in the numerical computations the Darcy equation should simply be rearranged to give the velocity in terms of permeability, viscosity and pressure gradients).

In crossflow filtration of suspensions the feed stream which flows adjacent to a porous wall is not a clear fluid and carries solid particles. As the filtration progresses due to the migration of these particles the rheological behaviour of the feed stream fluid changes with time and position. Therefore, a flow model which is limited to Newtonian fluids cannot be expected to provide an adequate representation of the flow field in crossflow filtration and the scheme should be able to simulate non-Newtonian (non-linear) flow behaviour. In the present scheme, the generalised Navier–Stokes equations are used to represent the feed stream flow. To cope with the non-linearity of these equations, a local (nodal) iteration procedure is included in the developed scheme which is used to update the nodal values of viscosity. In the examples given in this work, the nodal viscosities are found using a power-law constitutive equation. If it is desired, this equation can easily be substituted by a different constitutive relationship which gives a closer account of the rheological behaviour of a feed stream fluid. Depending on the availability of an appropriate equation of state a similar procedure can also be used to update the nodal values of the fluid density.

COMPUTATIONAL RESULTS

The flexibility of the developed technique allows it to be used either simply as a method to impose permeable wall conditions in a viscous flow domain or it can be applied to model the entire flow regime in a shell and tube system. Therefore in the present work two cases are considered.

In the first problem the flow of water in an axisymmetric annulus of 0.5 m length and inner radius of 0.02 m and outer radius of 0.07 m is simulated. A section in the middle of the inner wall is porous and the rest of this boundary and the entire outer shell are non-slip solid walls. The length of the porous section is 0.38 m. At the inlet a plug flow with a velocity of 0.02 m/s is given as the boundary condition. The convective acceleration terms for this flow are significant and it should be treated as a non-creeping incompressible laminar axisymmetric Newtonian regime governed by the Navier–Stokes equations. Due to the existence of a non-permeable section at the end of the domain the prescription of the developed flow or standard stress free conditions at the exit can be regarded as a reasonable choice in this problem. It should, however, be noted that a better approximation may be needed in more complex problems. More explanations regarding the choice of exit conditions in shell and tube flow systems is given later in this section. For a fully open exit the simulated flow fields with porous wall permeability of 10^{-8} and 10^{-7} m² (in the radial direction, no axial flow along the porous wall is assumed) are shown in Figs 1 and 2, respectively. These results are computed on a finite-element mesh of 128 nine-noded bi-quadratic C^0 elements. The steady-state solution is obtained after a minimum of 12 iteration cycles. However, more accurate solutions are obtained if steady state is approached slowly by increasing the number of these cycles (i.e. the number of corresponding predictor–corrector steps). The increase in permeability has a very significant effect on

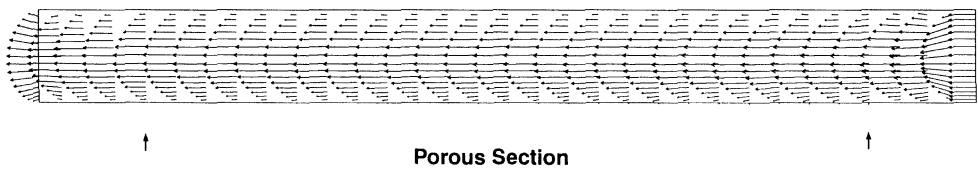


Fig. 1. Velocity field in a fully open exit annulus with a porous inner wall with a radial permeability of 10^{-8} m² (velocity vectors and the domain are plotted using different scales).

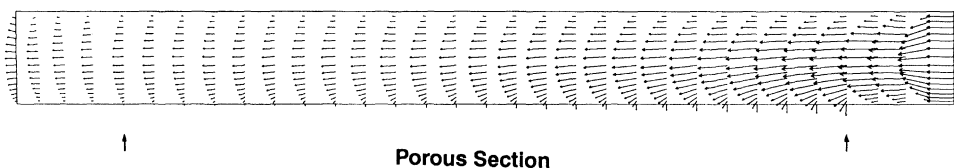


Fig. 2. Velocity field in a fully open exit annulus with a porous inner wall with a radial permeability of 10^{-7} m² (velocity vectors and the domain are plotted using different scales).

the amount of seepage flow through the porous boundary. The amount of flow passing through the porous wall (porous inner surface of the annulus) is found by

$$Q_p = 2\pi r_i \int_{z_1}^{z_2} v_r dz \tag{14}$$

where r_i is the inner radius of the annulus and z_1 and z_2 are the axial coordinates of the beginning and end of the porous section, respectively. The amount of outflow is found by

$$Q_o = 2\pi \int_{r_i}^{r_o} v_z r dr \tag{15}$$

where r_o is the outer radius of the annulus. The integrals in eqs (14) and (15) are found numerically using finite- element interpolation to represent axial or radial velocities (Nassehi and Petera, 1994). The ratio of permeate flow to the discharge through the exit drops from 8 to 0.6 by reducing the permeability from 10^{-7} to 10^{-8} m². The overall material balance based on the comparison of total inlet flow with the sum of permeate and outflows in both cases shows the accuracy of the numerical simulations. For wall permeability of 10^{-8} m² the difference between input and the total output is less than 1%. The discrepancy between the inlet and the total exit flows in the case of increased permeability is slightly higher than the lower permeable wall but it is only 2.5%.

The presented results are obtained using a coarse mesh and it is expected that even more accurate simulations can be produced if finer meshes are used. Furthermore, the accuracy of the present simulations

are significantly improved if the time step in the successive predictor–corrector calculations is made smaller, i.e. the number of transient stages leading to the steady state is increased. Numerical experiments showed that, in the above problem using the same mesh, the difference between the input and the total output is reduced to 2.3% if the steady state is approached more gradually after 14 intermediate transient stages instead of 12. An additional increase in the number of cycles from 14 to 18 further improves the accuracy of this simulation and the overall mass balance error drops to 1.7%.

The pressure contour plot corresponding to the flow field with wall permeability of 10^{-7} m² is given in Fig. 3 which, as expected, shows some deviation from a typical pressure field for simple pipe flow characterised by equidistant parallel contours. In order to investigate the effect of exit conditions the flow regime in a partially closed end annulus is simulated. The simulated flow field for wall permeability of 10^{-7} and 10^{-8} m² are shown in Fig. 4 and 5, respectively. In these simulations the stress free outflow conditions are used. The errors in overall mass balance in these simulations are 4.1 and 2.8% using 12 predictor–corrector steps. The increase in the discrepancy between the inlet flow and the sum of permeate and exit flows, in comparison to the fully open end case, is mainly due to the use of approximate exit boundary conditions (Griffiths, 1997). Pressure contours corresponding to the velocity field shown in Fig. 5 are given in Fig. 6. This graph shows an expected increase in the pressure gradient along the free flow direction as a result of lower porous wall permeability.

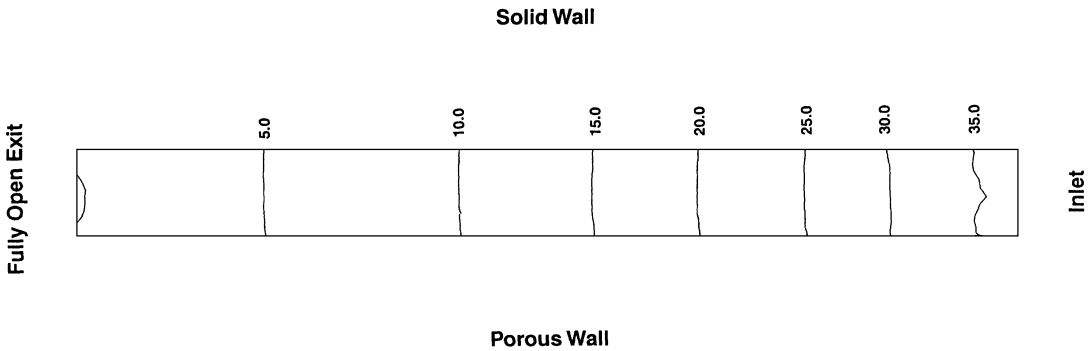


Fig. 3. Pressure contours corresponding to the velocity field shown in Fig. 2.

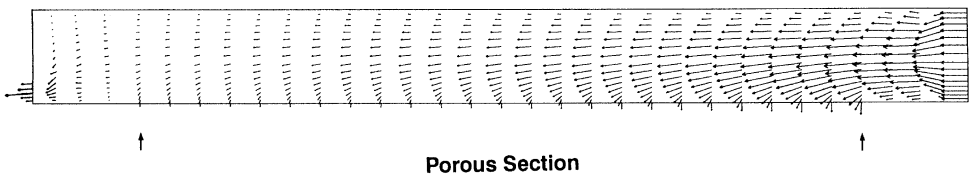


Fig. 4. Velocity field in a partially open exit annulus with a porous inner wall with a radial permeability of 10^{-7} m² (velocity vectors and the domain are plotted using different scales).

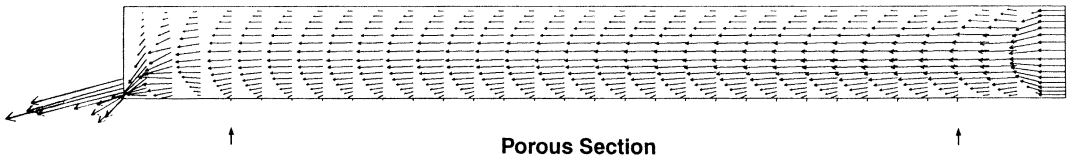


Fig. 5. Velocity field in a partially open exit annulus with a porous inner wall with a radial permeability of 10^{-8} m^2 (velocity vectors and the domain are plotted using different scales).

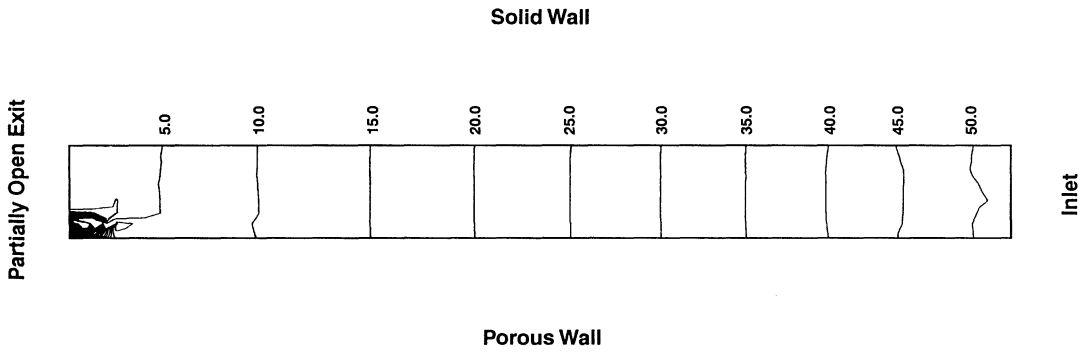


Fig. 6. Pressure contours corresponding to the velocity field shown in Fig. 5.

In the second problem considered in the present study, a complete shell and tube system of 0.5 m length, inner radius of 0.02 m, outer radius of 0.06 m and porous wall thickness of 0.005 m is modelled. Initially, the flow and seepage of water in this system was simulated and the overall mass balance was checked. The model results showed 4% discrepancy between the inlet flow and the total outflows through the outer shell and inner tube exits if steady state achieved after 12 cycles. The successive applications of

the predictor–corrector steps was increased to 18 steps and the mass balance error was reduced to 1.9%. Following this test a more complex flow problem was investigated. In this problem the feed stream consists of a slurry defined as a power-law fluid of density, $\rho = 1825 \text{ kg/m}^3$, consistency coefficient of $\eta_0 = 0.83$ and index $n = 0.64$. The permeate is water. The solution mesh therefore represents the inner tube from axis of symmetry to the inside surface of the annulus, porous wall and the outer shell. The flow

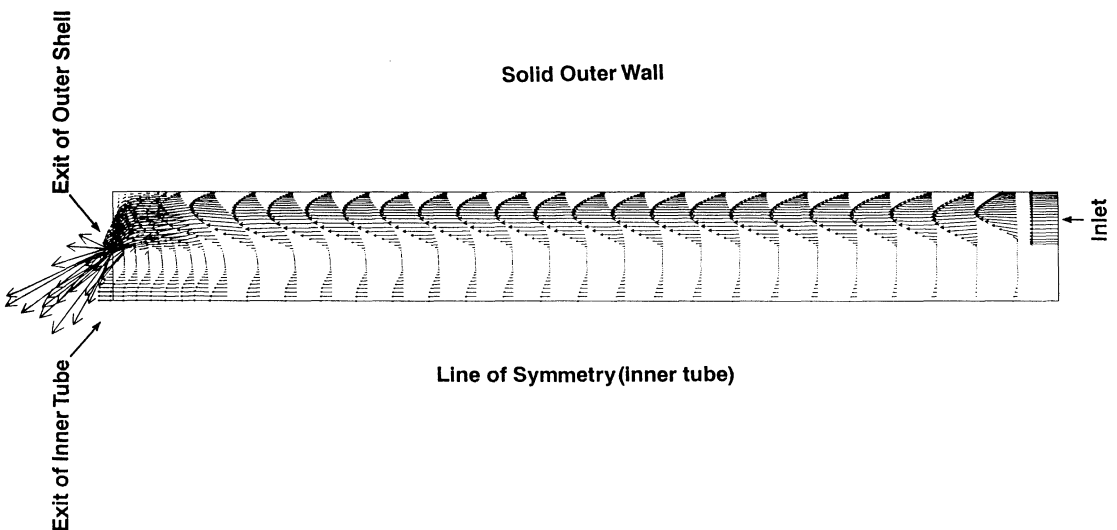


Fig. 7. Velocity field in a shell and tube system with inner tube wall permeability of $3 \times 10^{-6} \text{ m}^2$ in the radial direction. The axial permeability of the inner tube wall is zero.

regime is described as laminar, non-creeping incompressible non-Newtonian flow in the outer shell, incompressible seepage Newtonian flow through the wall and laminar, and non-creeping incompressible Newtonian flow in the inner tube. Inlet is through the outer shell.

Two different situations are investigated. In the first case, the exit from the outer shell is partly blocked and the inner wall permeability in the radial direction (i.e. k_r) is given as $3 \times 10^{-6} \text{ m}^2$. It is assumed that the inner wall is impervious in the axial direction. This is the normal situation in track-etched membranes. The imposed boundary conditions are zero velocity along the outside wall of the shell, known plug flow inlet velocity (0.01 m/s), conditions of symmetry (i.e. $v_r = 0.0$) along the inner tube axis. At the exit to avoid approximations generated by the use of unrealistic stress-free conditions the 'free boundary conditions' suggested by Papanastasiou *et al.* (1992) is used. This means that the line integrals generated by the application of the Green's theorem in the weighted residual statement of the problem which correspond to the nodes located at the exit are not eliminated by the imposition of artificial stress-free conditions and instead they remain in the elemental equations and should be treated as unknowns. Renardy (1997) has shown that a more suitable exit boundary condition for discretised flow equations can be imposed in this manner. In practice, a first guess solution based on the imposition of the standard outflow boundary conditions is found and used to obtain better results by the described method via an iterative cycle. It should be noted that this method is only relevant to free exits from a flow domain and it cannot be used in the case of exit by seepage through a porous wall. In the present work, in order to simulate the flow in the described shell and tube system in the layers of elements which join the free flow to the seepage flow regimes the terms of elemental equations which correspond to the nodes located on the porous surface are modified according to the technique described in this paper. The predicted steady-state flow field in this case is shown in Fig. 7 and it seems to be accurate in every respect. A previous model, based on the use of mathematically sophisticated C^1 continuous isoparametric Hermite elements for linking Navier–Stokes and Darcy equations, generated spurious circulations in the flow field under exactly the same conditions as in this example (Nassehi and Petera, 1994). This comparison provides an indication for the robustness of the present model. Figure 7 shows the velocity profile in the outer shell region, through the porous wall and inside of the inner tube. The pressure contours corresponding to this flow system are given in Fig. 8. These isobars show a continuous pressure drop from the outer shell to the inner tube across the membrane.

As a numerical experiment the velocity and the pressure data found for the porous region in this example were inserted in the Brinkman equation. The aim was to estimate the equivalent 'effective viscosity'

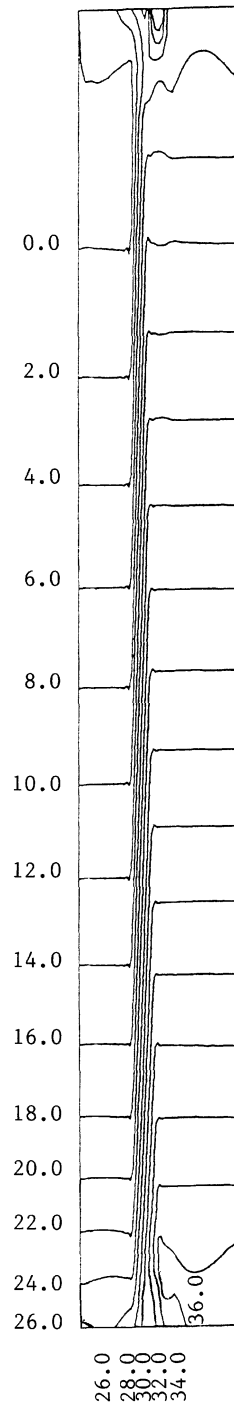


Fig. 8. Pressure contours corresponding to the velocity field shown in Fig. 7.

which can give comparable flow field results if the Darcy equation is replaced by the Brinkman model in this simulation. This experiment gives a μ^* which is approximately 10–15 times smaller than the true permeate viscosity at different sampling nodes inside the porous region. This is not unexpected since the insertion of μ^* values which are smaller than the true viscosity renders the second-order term in the

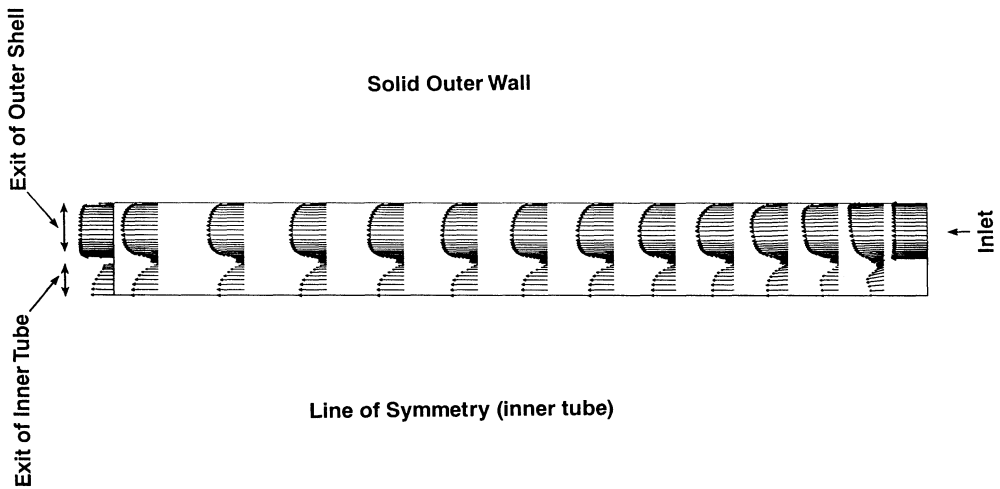


Fig. 9. Velocity field in a shell and tube system with inner tube wall permeability of $3 \times 10^{-6} \text{ m}^2$ in the radial direction. The axial permeability of the inner tube wall is 10^{-9} m^2 .

Brinkman equation insignificant and hence it becomes closer to the Darcy model.

In the second shell and tube system simulated in the present work the exit from the outer shell is fully open. Also in addition a membrane which is permeable in both radial and axial directions is considered. Here, the radial and the axial permeability coefficients of the inner tube wall (i.e. k_r and k_z) are, respectively, given as 3×10^{-6} and 10^{-9} m^2 . The membrane wall at the exit from the flow domain is assumed to be solid and along this line both coefficients are given as zero. The simulated flow field in this case is shown in Fig. 9. This figure indicates that, under the given conditions, the velocity field in the inner tube tends to become almost parabolic and it is nearly constant after a short distance from the inlet. This changes, abruptly, at the exit since the insertion of zero permeability stops the flow through the porous wall and significantly alters the velocity profiles in both regions. As it can be seen in Fig. 9, tangential velocities on the surface of the porous wall can be simulated by the present scheme. Therefore, the developed model can be used as a tool to generate porous flow fields comparable with the model suggested by Beavers and Joseph (1967). These investigators postulated the existence of a slip velocity along the surface of the porous section in order to give an analytical account of experimentally obtained mass efflux of viscous fluids in porous domains. It is however, important to note that in the present scheme the insertion of a non-zero permeability in the axial direction, which results in the appearance of a slip velocity on the porous surface, does not mean that the shear stresses across interfacial boundary between the flow regions are made continuous. The possibility of the matching of the shear stresses across the boundary between free and porous flow regimes is often cited as a rationale for using the Brinkman model instead of the Darcy equation in

porous flows. However, in combined flow systems, matching of the shear stress on the sides of the interface between free and porous regions cannot be regarded as valid since, on the porous side, a portion of the stress is carried by the solid matrix (Nield and Bejan, 1992). The pressure contours corresponding to the velocity field given in Fig. 9 are shown in Fig. 10. The pressure isobars shown in Fig. 10 reflect the special form of the simulated flow field given in Fig. 9. As the velocity profile inside the inner tube tends to become constant the pressure gradient in the axial direction in this region almost vanishes. This can be contrasted with the simulated pressure field shown in Fig. 8 which reflects the change of the velocity profile along the entire length of the inner tube.

CONCLUSION

In this paper a new method for the imposition of permeable wall conditions in viscous flow domains is presented. This method offers a general technique for the linking of the free flows modelled by the Navier–Stokes equations to flow through permeable walls described by the Darcy equation. In the present study the developed technique has been applied to model the combined flow of feed stream and permeate in axisymmetric shell and porous tube systems. This configuration is widely used in many crossflow filtration processes in industry and accurate modelling of the flow regime in these systems is a basic requirement in the development of reliable predictive filtration models. Thus, the present combined Navier–Stokes/Darcy flow model can be regarded as the first step towards creating a complete model for crossflow filtration. Such a task will involve the application of the present model in conjunction with appropriate species transport (e.g. particle migration in suspensions) and constitutive and state equations which take into

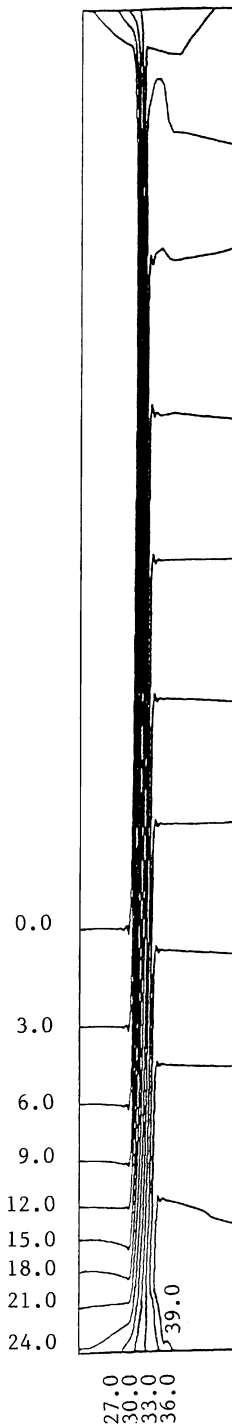


Fig. 10. Pressure contours corresponding to the velocity field shown in Fig. 9.

account the variations of fluid properties. The computational results obtained by the described method show that the model accurately preserves the flow continuity in complex branching flow domains. Various simulations based on different inlet velocity profiles, wall permeability and exit conditions are presented to show the flexibility of the developed scheme.

NOTATION

a_{lm}	member of coefficient matrix in the elemental working equation
b_l	member of load vector in the elemental working equation
c	speed of sound in the fluid
g_r, g_z	components of the body force vector
K, K_r, K_z	Darcy permeability, non-isotropic Darcy permeability in r and z directions
n	power-law index
n_r, n_z	components of the unit normal vector
N_m	interpolation function associated with node m
N_l	weight function number l
p, p^e	pressure, interpolated pressure
t	time variable
$v_r, v_z;$ v_r^e, v_z^e	velocity components, interpolated velocity components
$r, z; r^e, z^e$	space variable, interpolated spatial variables used in iso-parametric elements

Greek letters

$\dot{\gamma}$	shear rate
η	shear-dependent viscosity of a power-law fluid
η_0	consistency coefficient (zero shear rate viscosity) of a power-law fluid
μ, μ_f, μ^*	Newtonian viscosity, viscosity of the filtrate, effective viscosity
ρ	fluid density

REFERENCES

- Beavers, G. S. and Joseph, D. D. (1967) Boundary conditions at a naturally permeable wall. *J. Fluid Mech.* **30**, 197–207.
- Bowen, W. R., Mongruel, A. and Williams, P.M. (1996) Prediction of the rate of cross-flow membrane ultrafiltration: a colloidal interaction approach. *Chem. Engng Sci.* **51**, 4321–4333.
- Brinkman, H. C. (1947) A calculation of the viscous force exerted by a flowing fluid on a dense array of particles. *Appl. Sci. Res.* **A1**, 27–34.
- Durlofsky, L. and Brady, J. F. (1987) Analysis of the Brinkman equation as a model for flow in porous media. *Phys. Fluids* **30**, 3329–3341.
- Gartling, D. K., Hickox, C. E. and Givler, R. C. (1997) Simulation of coupled viscous and porous flow problems. *Int. J. Comput. Fluid Dyn.* **7**, 23–48.
- Givler, R. C. and Altobelli, S. A. (1994) A determination of the effective viscosity for the Brinkman-Forchheimer flow model. *J. Fluid Mech.* **258**, 355–370.
- Griffiths, D. F. (1997) The ‘no boundary condition’ outflow boundary condition. *Int. J. Numer. Methods Fluids* **24**, 393–411.
- Gutman, R. G. (1987) *Membrane Filtration*. Adam Hilger, Bristol, U.K.
- Kaviany, M. (1991) *Principles of Heat Transfer in Porous Media*. Springer, New York, U.S.A.
- Kim, S. and Russell, W. B. (1985) Modeling of porous media by renormalization of the Stokes equations. *J. Fluid Mech.* **154**, 269–286.

- Lundgren, T. S. (1972) Slow flow through stationary random beds and suspensions of spheres. *J. Fluid Mech.* **51**, 273–299.
- Martys, N., Bantz, D. P. and Barboczi, E. J. (1994) Computer simulation study of the effective viscosity in Brinkman's equation. *Phys. Fluids* **6**, 1434–1439.
- Nassehi, V. (1996) Generalised Hele–Shaw models for non-Newtonian, non-isothermal flow in thin curved layers. *IMA J. Math. Appl. Business Industry* **7**, 71–88.
- Nassehi, V. and Bikangaga, J. H. (1993) A mathematical model for the hydrodynamics and pollutants transport in long and narrow tidal rivers. *Appl. Math. Modelling* **17**, 415–422.
- Nassehi, V. and Petera, J. (1994) A new least-squares finite element model for combined Navier–Stokes and Darcy flows in geometrically complicated domains with solid and porous boundaries. *Int. J. Numer. methods Engng* **37**, 1609–1620.
- Nassehi, V. and Petera, J. (1997) Mathematical modelling of flow characteristics in cross-flow filtration and design of efficient micro-filters. *Proceedings of the IChemE Jubilee Research Event*, pp. 1101–1104.
- Nield, D. A. and Bejan, A. (1992) *Convection in Porous Media*. Springer, New York, U.S.A.
- Pangrle, B. J., Alexandrou, A. N., Dixon, A. G. and Dibiasio, D. (1991) An analysis of laminar fluid flow in porous tube and shell systems. *Chem. Engng Sci.* **46**, 2847–2855.
- Papanastasiou, T. C., Malamataris, N. and Ellwood, K. (1992) A new outflow boundary condition. *Int. J. Numer. Meth. Fluids* **14**, 587–608.
- Petera, J. and Nassehi, V. (1996) Finite element modelling of free surface viscoelastic flows with particular application to rubber mixing. *Int. J. Numer. Meth. Fluids* **23**, 1117–1132.
- Reddy, J. N. (1986) *Applied Functional Analysis and Variational Methods in Engineering*. McGraw-Hill, New York, U.S.A.
- Reddy, J. N. and Gartling, D. K. (1994) *The Finite Element Method in Heat Transfer and Fluid Dynamics*. CRC Press Inc., Boca Raton, FL, U.S.A.
- Renardy, M. (1997) Imposing 'no' boundary condition at outflow: why does it work. *Int. J. Numer. Meth. Fluids* **24**, 413–417.
- Taylor, C. and Hood, P. (1973) A numerical solution of Navier–Stokes equations using FEM techniques. *Comput. Fluids* **1**, 73–100.
- Tucker III, C. L. (ed.) (1989) *Computer Modelling for Polymer Processing*. Hanser Publishers, Munich.
- Zienkiewicz, O. C. and Taylor, R. L. (1994) *The Finite Element Method, Vol. 1, 4th Edn*. McGraw-Hill, London, U.K.
- Zienkiewicz, O. C. and Wu, J., (1991) Incompressibility without tears-how to avoid restrictions on mixed formulation. *Int. J. Numer. Meth. Engng* **32**, 1189–1203.